Influence of the geometry of concrete aggregates on the CO_2 gas flow inside a carbonation reactor in an open system.

Kilesh JAUNKEYPERSAD, Johan COLIN, Adrien POUPARDIN, Jena JEONG
ESTP IR, 28 Av. du Président Wilson, 94230 Cachan

RESUME: The "CO_2 capture using the recycled concrete aggregate" research program has been established to conceptualize a reactor as part of the national research program, Fastcarb. However, understanding the complex interaction between gas mixture ($CO_2 + N_2$) flow patterns, heat transfer phenomena and reaction in a porous media (carbonation) is very crucial for optimizing the performance of the reactor to maximize CO_2 capture. The study presents a comprehensive numerical investigation into the coupling of fluid flow and heat transfer phenomena within the reactor. The analysis uses the Computational Fluid Dynamics (CFD) technique to assess the thermal performance and fluid dynamics characteristics of the carbonation reactor while varying the shape and number of aggregates. The results provide valuable insights into a deeper understanding of the gas flow and heat distribution in the reactor, which could help optimize the carbonation of concrete aggregates. Additionally, the vorticity results around the concrete aggregates provide insight into the zone most likely to undergo carbonation, and the 'dead zone' where any CO2 gas would not interact with the concrete aggregate.

Keywords: CO_2 gas flow, Heat transfer, Multiphysics CFD, and carbonation reactor

I. INTRODUCTION

The need to mitigate climate change has intensified research programs in CO_2 capture and storage. In this perspective, the national research "Fastcarb" has been put in place which aims to recycle concrete waste through the capture of CO_2 gas by conceptualizing a carbonation reactor as it emerges as a promising tool for efficiently capturing CO_2 from diverse sources, including cement factories and other industries (Schmitt et al., 2022). Precisely the goal is to use the RCAs (Recycled Concrete Aggregate) to capture the industrial CO_2 gas. In the previous contribution (Jeong et al., 2022) , the CO_2 sequestration capacity of recycled concrete aggregate was investigated by both 3D numerical simulations and experiments. The numerical simulation of carbonation using reactive transport modeling was utilized in CO_2 storage assessments through a spherical geometry in Figure 1A.

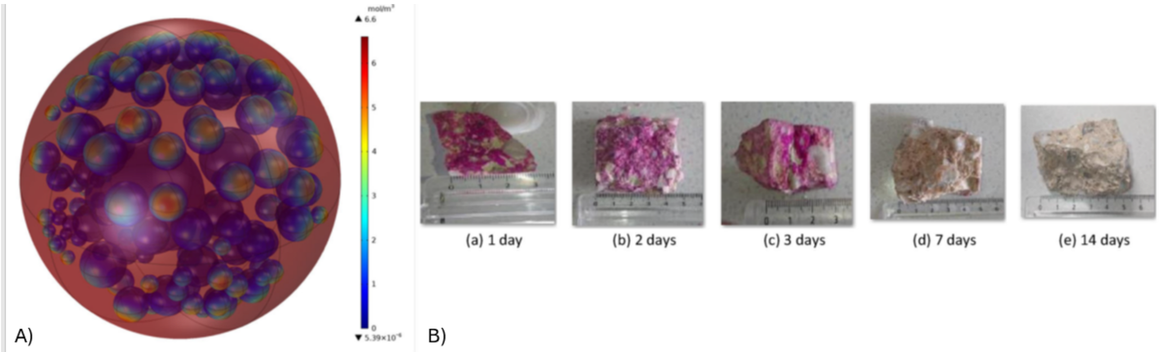

Figure 1 : Illustration of CO_2 diffusion in the two-phase numerical model (A) and presentation of CO_2 carbonation stages for the concrete aggregates from 1 day to 14 days after carbonation in an incubator.

We have computed the mass of CO_2 gas reacted with cement components as a function of time obtained on the samples shown in Figure 1B. This modelling also provides the CO_2 gas concentration ready to be used for the carbonation reactions in the pores. We also concluded that the numerical modelling well agrees with the experiments. However, the carbonation method in an incubator is designed for laboratory-scale experiment, not for an industrial-scale carbonation reactor tested during the project Fastcarb, which utilizes an open and continuous reactor system. The laboratory-scale experiment uses an incubator filled with CO_2. This involves a closed system with no CO_2 gas flow around the sample, and therefore, the boundary condition remains constant regardless of the shape, size, or duration of carbonation. This method does not meet the requirements for industrial-scale carbonation. The current study aims to comprehend the experimental condition of CO_2 gas flow for the carbonation of concrete aggregates through numerical simulation, and we focus on the continuous system of a reactor that we established in our laboratory to mimic the industrial gas condition which is proposed for the "Fastcarb" national project. Indeed, gas, aggregates, and their features need to be taken into consideration, dealing with the hot gas (20 °C ≤ T ≤ 100 °C) and gas type. And concerning the aggregates consideration should include geometry, water content, and the quantity of cement paste. Therefore, understanding carbonation kinetics in a reactor is not as easy as it appears because it involves multi-physical phenomena. That is why it is important to study the flow behavior and heat transfer inside the reactor and diffusion-reaction process in the concrete aggregates. This paper aims at examining the flow pattern, the velocity distribution and lastly the temperature distribution within the reactor and then concrete aggregates.

In general, there are two types of reactors, one of which operates on an industrial scale and the other is designed for laboratory-scale experiments as shown in Figure 2 . In the "Fastcarb" project, two reactors were also proposed at an industrial scale (Torrenti et al., 2022) but unfortunately, no proper theoretical or experimental investigation was carried out to justify their configuration. In alignment with recent advancements in gas flow optimization, the authors (Mehdipour et al., 2020), extensively explored three different gas flow configurations in a reactor for the carbonation of a concrete block, showing how the configuration of the gas flow impacted the CO_2 uptake. In another study, Minhua et al. (2019) and Wen & Ding (2006) conducted comprehensive Computational Fluid Dynamics (CFD) studies, emphasizing an in-depth analysis of flow behavior, heat transfer, and reaction-diffusion processes. Their research enhances understanding of fluid dynamics within a fixed-bed reactor through detailed computational modeling. Consequently, it revealed the disadvantage of having a fixed bed which resulted in heterogeneous results.

Figure 2 : (A) laboratory-scale reactor (Lombardi et al., 2016) ; (B) industrial scale reactor (Schnabel et al., 2021) (C) Carbonation reactor in our laboratory at ESTP.

II. LABORATORY-SCALE CARBONATION REACTOR.

The reactor as shown in Figure 2C was set up to conduct carbonation tests with a 15 % CO_2 flux as part of the Fastcarb project. Following inconclusive results with very poor rate of fixed CO_2 at a higher temperature between 40 °C ≤ T ≤ 60°C following the blue cross and red circles as shown in Figure 3A, we decided to assess the reliability of our reactor, specifically the gas heating system through an experimental approach. The experiment consisted of measuring the temperature at the top and the bottom of our reactor and that of the concrete aggregate. The placement of the heating element inside the reactor resulted in the temperature heterogeneity between the top and bottom of the reactor as well as that of the concrete aggregate as we can observe in Figure 3B.

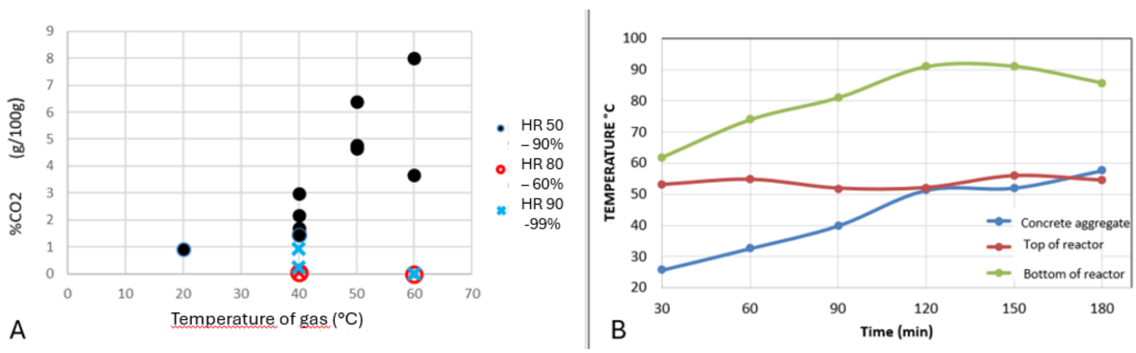

Figure 3 : A) Results of carbonation test at high temperature (40 °C ≤ T ≤ 60°C); B) Temperature difference between the top and bottom of reactor and that of concrete aggregate.

So, as our temperature probe was placed at the top of the reactor it would register only the temperature at the top, giving us the wrong indication for temperature reading thus falsifying all our results. To overcome this problem, we decided to the heating configuration of our reactor. Meanwhile, we investigate 3D CFD modeling to understand the flow of the CO_2+N_2 gas mixture inside the reactor and its path around the aggregates.

III. MULTIPHYSICS CFD MODEL

In this section, we simulate 3D CFD model inspired by our new heating configuration, by combining fluid flow of two gases (CO_2 + N_2) and heat transfer as this paper aims to bridge existing gaps concerning the factors influencing CO_2 uptake such as reactor design (gas flow configuration) and operational conditions (fluid flow and heat transfer). Afterward, these case studies are going to be numerically tested at various number of spherical concrete aggregates.

A. Governing equations for fluid flow and heat transfer in fluid and solid

Our exploration into fluid dynamics is based on a foundation of incompressible Newtonian fluids that is the Navier-Stokes equations (Gunzburger, 1996). First formulated in 19th century by Claude-Louis Navier and George Gabriel Stokes, these equations enclosed the fundamental principles of underlying fluid flow.

Continuity equation for incompressible flow :

$$\nabla . V = 0 \qquad (Eq\ 1)$$

Momentum equations for incompressible Newtonian fluids :

$$\frac{\partial V}{\partial t} + (V . \nabla)V = -\frac{1}{\rho}\nabla p + v\nabla^2 V + F \qquad (Eq\ 2)$$

Here, V is the velocity vector, ρ is the fluid density, p is the pressure, v is the kinematic viscosity, and F represents any external forces acting on the fluid. The flow is characterized in our case as an incompressible flow with the ratio of gas velocity to the speed of sound approximately equal to 0.00897 which fully satisfies the criteria of an incompressible flow with Mach number < 0.3 as shown in Table 1 .

Table 1 : Flow classifications in terms of Mach number.

Mach number	Flow regime	Density gradient
Ma ≤ 0.3	Incompressible	Negligeable
0.3 < Ma ≤ 0.8	Subsonic	Small
0.8 < Ma ≤ 1.2	Transonic	Significant
1.2 < Ma ≤ 3,0	Supersonic	Significant
Ma > 3.0	Hypersonic	Dominant

The continuity equation (Eq 1) reinforces the assumption of incompressible flow, satisfying the fact that the divergence of the velocity vector V must be zero. In practice, this assumption is valid when fluid density remains unchanged allowing us to focus on the essential dynamics of flow as in our case. As for the momentum equations (Eq 2), it is tailored for fluids that resist compression and describe the motion of the fluid element. On the left-hand side, we have the acceleration of fluid particles, while the right-hand side comprises the pressure gradient force, viscous effects, and any external forces (F) acting on the fluid. The term v reflects the kinematic viscosity of the fluid, a parameter intrinsic to its Newtonian behavior. The heat equation involving convection is given in the form below offering a comprehensive framework to analyze how thermal energy propagates through a fluid medium. The governing heat equation is expressed as:

$$\rho C_p \frac{\partial T}{\partial t} + \rho C_p u \,.\, \nabla T + \nabla \,.\, q = Q \qquad (Eq\ 3)$$

Where, $\rho C_p \frac{\partial T}{\partial t}$ signifies the rate of change of internal energy per unit volume with Cp representing the specific heat capacity of the fluid and $\frac{\partial T}{\partial t}$ denotes the rate of change of temperature to time. And the term $\rho C_p u \,.\, \nabla T$ in (Eq 3) accounts for the advective transport of internal energy. Where u is the velocity vector of the fluid and ∇T represents the temperature gradient.

$\nabla \,.\, q$ where $(q = -k\nabla T)$ reflects the divergence of the heat flux vector and in other words describe how heat is conducted within the fluid. Finally, Q in (Eq 3) represents the heat source and also external factors affecting the energy balance.

B. Multiphysics CFD modeling condition and numerical bed of spherical concrete aggregates and CO2 reactor.

In Figure 4, we have an overview of the 3D model with our cylindrical reactor (of ⌀ = 380 mm and height 380 mm) and a spherical concrete aggregate (of ⌀ = 20 mm) with the gas inlet and outlet. The hot gas mixture of (CO_2 + N_2) enters the reactor through the gas inlet (of ⌀ = 10 mm) and passes through the sphere until reaching the gas outlet (of ⌀ = 10 mm). The various simulation parameters are listed in Table 2.

Table 2 : Simulation parameters

	Gas		Reactor	Concrete aggregate	Air
	CO_2	N_2			
Temperature (K)	323	323	293,15	293,15	293,15
Velocity (m/s)	0.35	2.34	-	-	-
Thermal conductivity W/(m.K)	0.0162	0.0258	-	1.8	0.0257
Heat capacity	844.2	1039	-	880	1005

J/(kg.K)					
Density (kg/m3)	1.842	1.165	-	2300	1.225
Pressure	1 [atm]	1 [atm]	1 [atm]	-	1[atm]

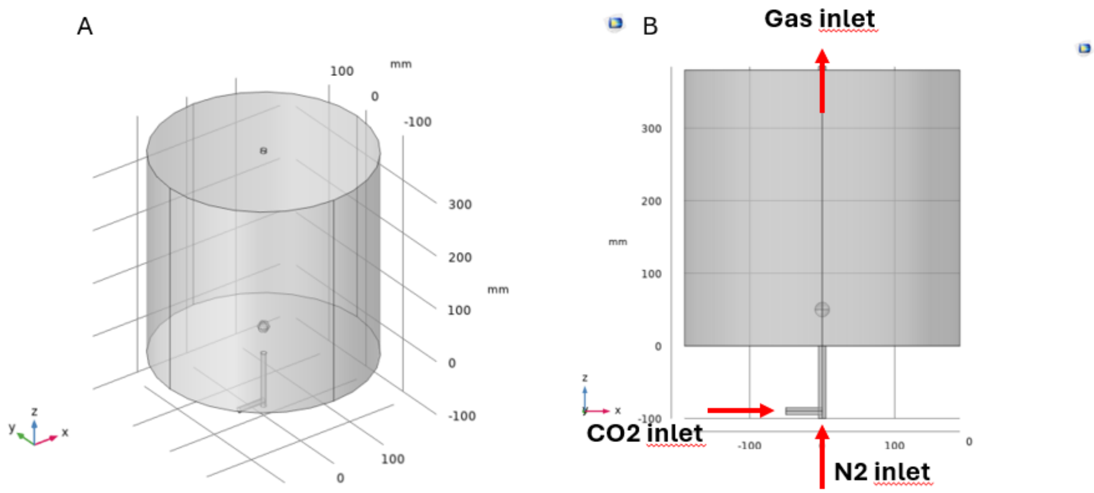

Figure 4 : (A) overview of 3D model (reactor + sphere) (B) Gas inlet and outlet.

The Multiphysics CFD simulation was performed in two steps: the first involves a bed of spherical concrete aggregates and the next one involves a two-bed configuration of spherical concrete aggregates. In the first case, the model was simulated at the scale of one spherical concrete aggregate. Afterward, the sphere is substituted with a real concrete aggregate. It aims to observe the influence of the geometry on the flow dynamics. Then, we proceeded with a layer of 9 spherical concrete aggregates and a bed composed of 81 spherical concrete aggregates. The arrangement and set-up of particles are shown in Figure 5.

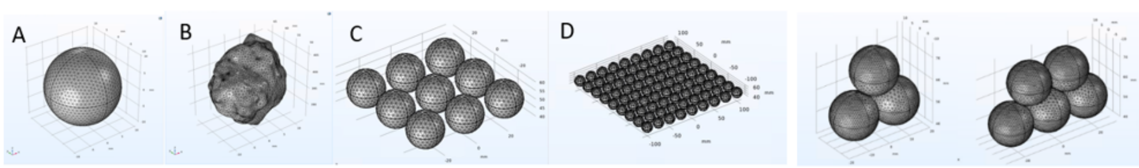

Figure 5 : A bed of spherical concrete aggregates (A,B,C, and D) and a two-layered configuration of spherical concrete aggregates (two right figures).

IV. RESULTS AND DISCUSSION

These simulations were conducted to understand the temperature distribution, and other key parameters in the reactor and around the concrete aggregate, for example, the vorticity, defined as a measure of the rotation of fluid particles within a fluid flow which indicates the tendency of fluid elements to spin or rotate around an axis, providing insight into the fluid's behavior, such as the formation of vortexes and turbulence, giving us an indication of the zones most likely to be in contact with the gas. The observations can hold particular significance in the context of optimizing the gas configuration of carbonation reactors in an open system, aiming to enhance the efficiency of capturing the CO_2 gas.

A. Results for one spherical concrete aggregate

By analyzing the results of flow or more precisely by visualizing the velocity field, a symmetrical flow pattern is observed due to the symmetrical shape of the sphere. However, beyond the limit of 10 seconds, a significant turbulence can be visually discerned in Figure 6B, persisting until the end of the simulation at 1800 seconds.

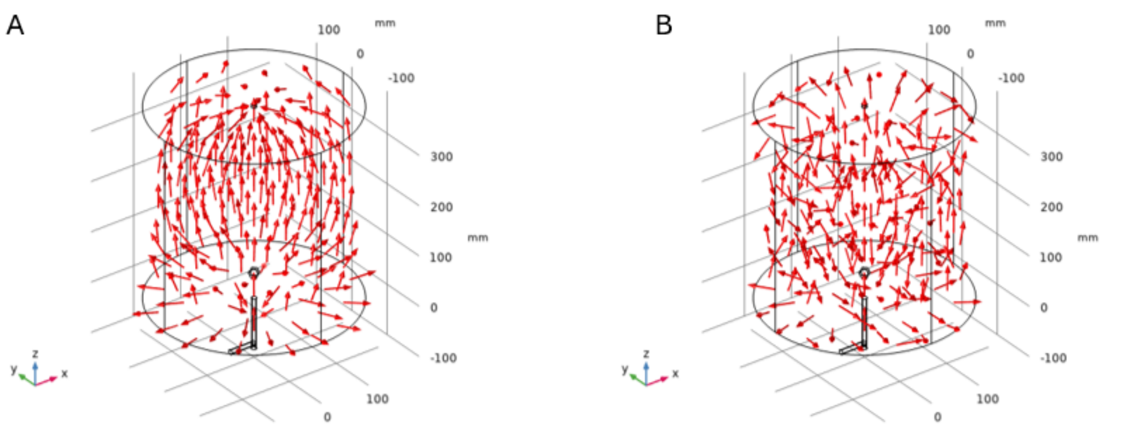

Figure 6 : Presentation of velocity field inside the reactor including one concrete aggregate ; A: velocity field at 10 s; B: velocity field at 1000 s.

Upon analyzing the flow pattern in terms of velocity distribution, a “dead zone”, defined as regions within a fluid flow where the velocity is significantly lower compared to the surrounding areas, where the flow may be stagnant or considerably slower, often leading to reduced mixing and potentially affecting the overall flow dynamics can identified at the back of our sphere as shown in Figure 7A, which corresponds to a zone of low pressure (4 – 5 Pa) and low velocity (0 – 0.5 m/s) as observed by (Minhua et al., 2019). These results remain unchanged even after 10 min of simulated time. Based on the results of vorticity, we can see clearly here how the dead zone can occupy around 50 % of the total surface area of the concrete aggregate. However, on the other hand, we can observe that the vorticity is spread on the sides of the concrete aggregate in Figure 7B. Essentially, this region is more favorable to carbonation as high vorticity regions ensures that the gas come into contact more frequently and in a more homogeneous manner with an increased surface area for reaction, which we assumed can lead to an increase in carbonation rate. To confirm our deduction, we have already prepared spherical-shaped mortar samples on which experiments will be conducted in the next study.

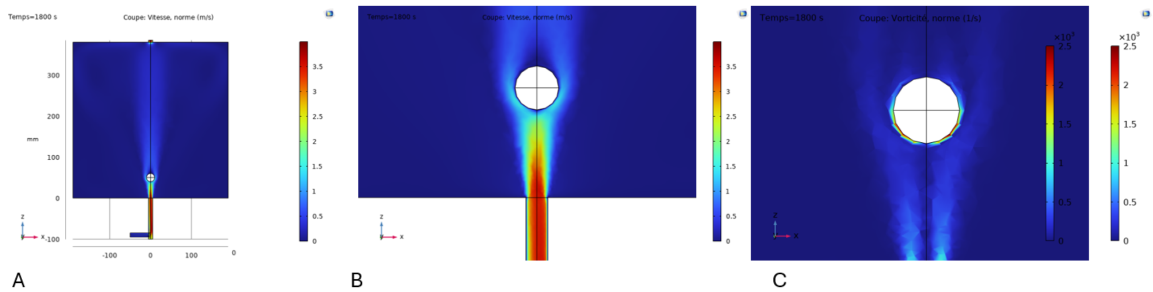

Figure 7 : A: Results of velocity (m/s) distribution in reactor and around the sphere at t = 10 min; B: Zoom on the spherical concrete aggregate showing the dead zone and the vorticity around the spherical concrete aggregate.

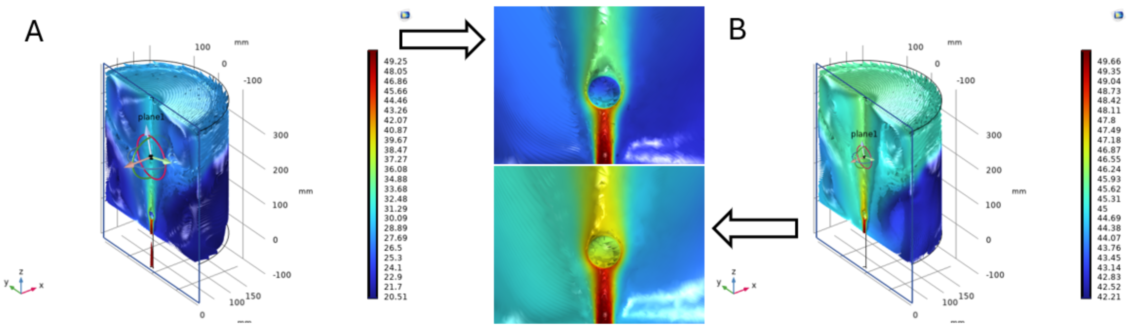

Figure 8 : A: Results of temperature (°C) distribution in the reactor and sphere at t = 1 min; B: Results of temperature (°C) distribution in the reactor and sphere at t = 10 min.

In Figure 8, we have the results of the heat distribution both within the reactor and the sphere at t = 1 min and 10 min respectively. It is noteworthy that within 10 minutes, thermal uniformity is achieved in both the reactor and the sphere. At the scale of one sphere, we can observe that there is not much difference in temperature between the sphere and the reactor by visualizing the zoomed image on the spherical concrete aggregate.

B. Results for one real concrete aggregate

For this simulation the sphere has been replaced by a real concrete aggregate in the model to see the impact of an irregular geometry on the fluid's dynamics. The numerical model of the concrete aggregate was obtained using Shining 3D Einscan-SP laser scan, which is available in our laboratory.

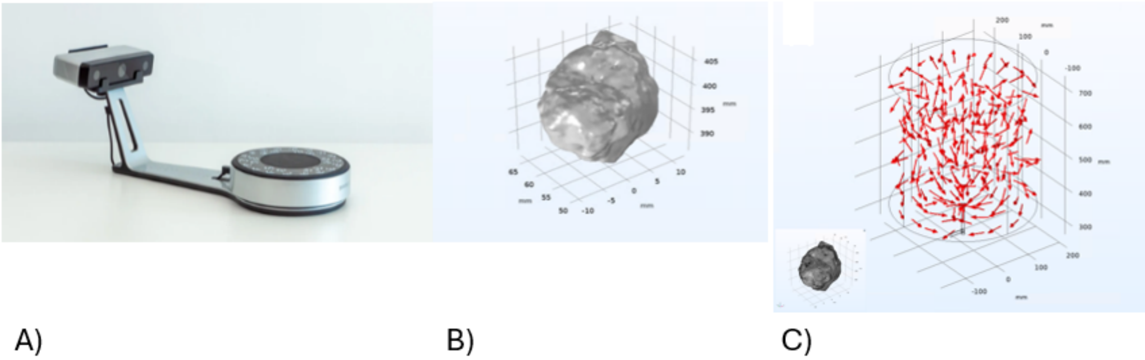

Figure 9 : A) Shining 3D Einscan-SP laser scan, B) real concrete aggregate : Surface 1347.1 mm² ; volume 3659.6 mm² C) velocity field at 10 s.

On analyzing the velocity field, it reveals the onset of turbulence in the flow during the first 10 seconds as we can observe in Figure 9C, in contrast to the spherical concrete aggregate where a relatively symmetrical pattern was observed in the first 10 seconds. The likely origin of this turbulence can be attributed to the irregular geometry of the real concrete aggregate. Over here an asymmetric flow pattern is observed, unlike in the case of a spherical concrete aggregate. Similarly, a dead zone can be identified at the back of the real concrete aggregate. We can observe in Figure 10B, that the dead zone extends to nearly 50 % of the total surface area of the real concrete aggregate. In contrast with the spherical concrete aggregate, we observed a higher and more widespread vorticity on the real concrete aggregate surface. Once again, we can witness the impact of the geometric effects, resulting in an increase in vortexes, in other words an increase in gas molecules interaction on the surface. This hypothesis still needs to be verified through experimentation. Regarding the temperature distribution, the model reaches 50 °C within the first 10 minutes, which is clearly faster than in the case of a spherical concrete aggregate. The explanation behind this is that the irregular geometry of the real concrete aggregate promotes a quicker heat distribution in the whole volume.

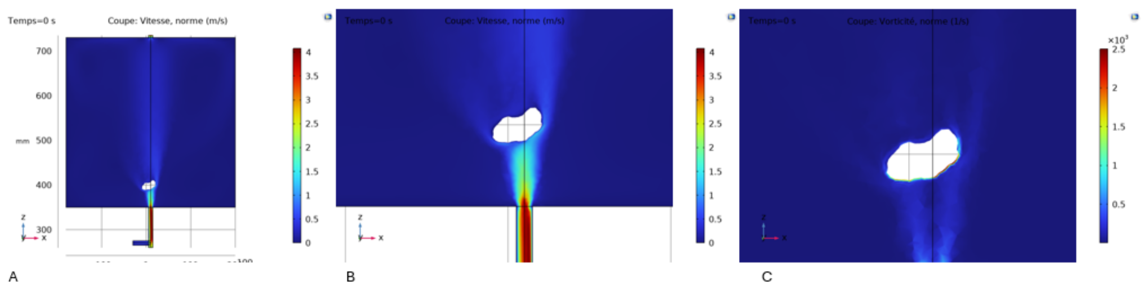

Figure 10 : A: Results of velocity distribution in reactor and around the real concrete aggregate at t = 1 min; B: Zoom on the real concrete aggregate showing the dead zone, and vorticity around the real concrete aggregate.

C. Results for a bed 9 and 81 spherical concrete aggregates

On the scale of a bed 9 and 81 spherical concrete aggregates, as expected, turbulence is observed within the first 10 seconds, and this pattern remains consistent until the end of the simulation as shown in Figure 11. The gas flow is not influenced since we have only one layer of particles with zero contact between them. According to Figure 12, we have the same scenario, which repeats as in the case of one spherical concrete aggregate. It is evident that the flow pattern is influenced only by the middle sphere in both cases. But for the neighboring sphere we can clearly observe that they do not even come in contact with the gas. Therefore, for a better understanding of the flow pattern we need to visualize the vorticity.

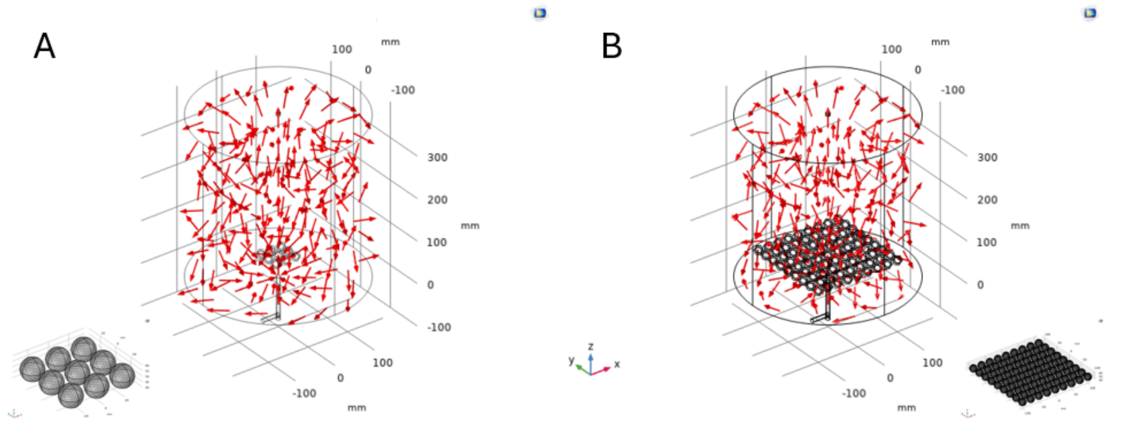

Figure 11 : A: velocity field at t = 10 s (9 spheres) B: velocity field at t = 10s (81 spheres)

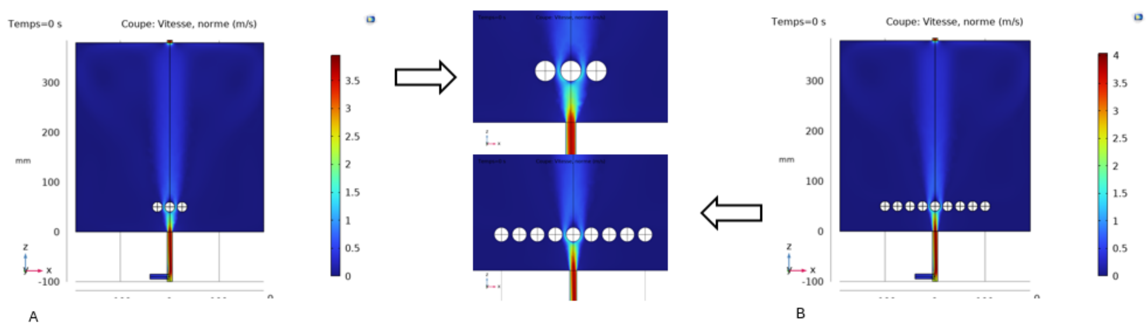

Figure 12 : A: Results of velocity distribution in reactor and around the spherical concrete aggregate for 9 spheres at t = 1 min with a zoom on the spheres on the right; B: Results of velocity distribution in reactor and around the spherical concrete aggregate for 81 spheres at t = 1 min

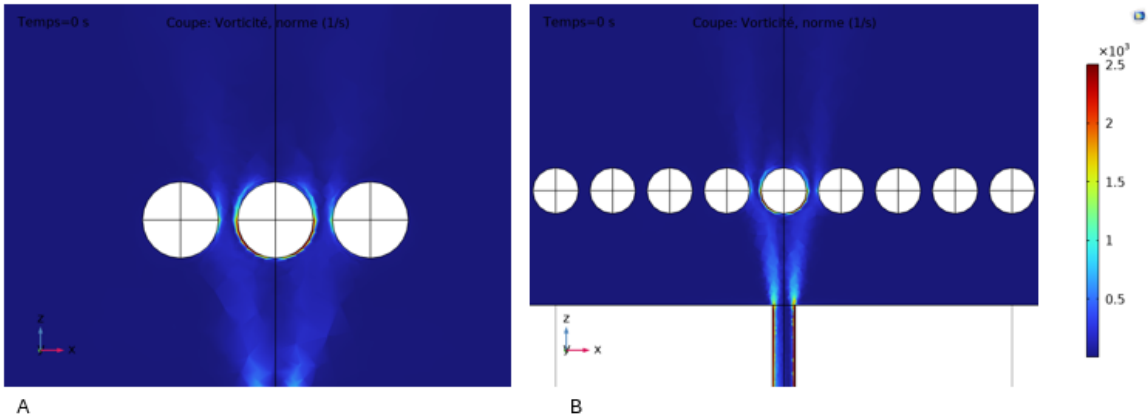

Figure 13 : A) vorticity (9 spheres), B) vorticity around the spherical concrete aggregates (81 spheres)

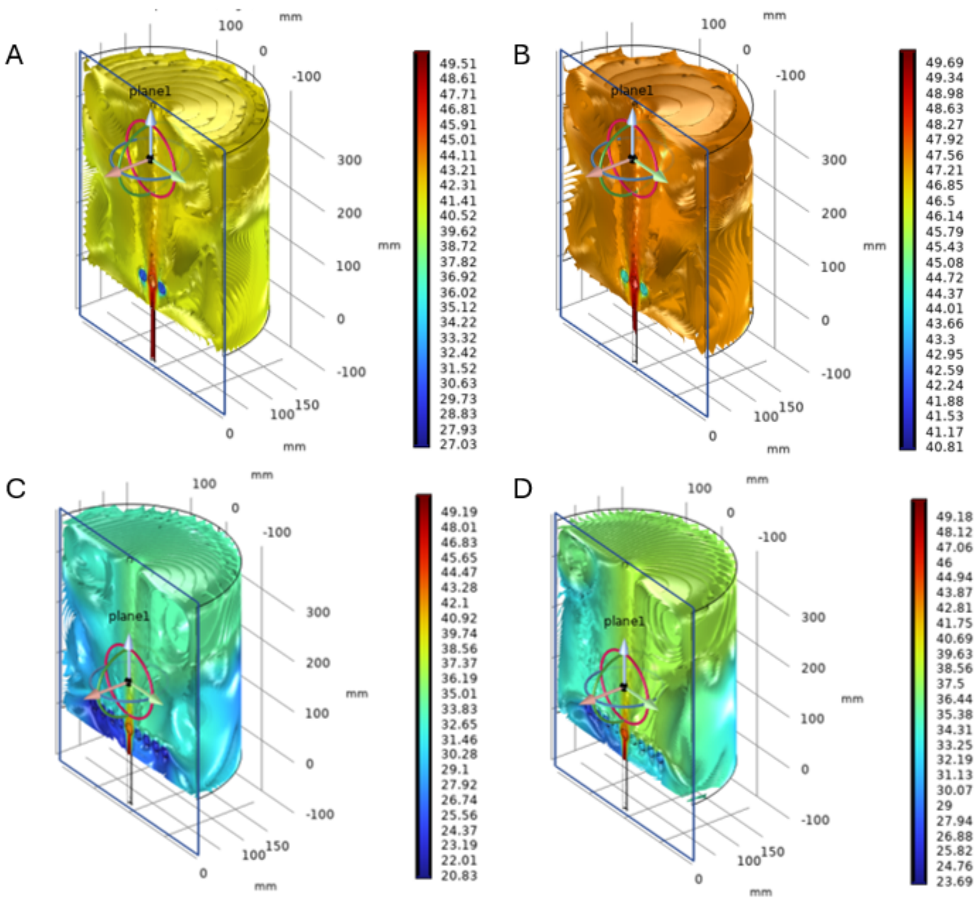

Figure 14 : A and B : Results of temperature (°C) distribution in the reactor and the spherical concrete aggregates in the case of 9 spheres at t = 10 min and t = 30 min respectively; C and D : Results of temperature (°C) distribution in the reactor and the spherical concrete aggregates in the case of 81 spheres at t = 10 min and t = 30 min respectively.

Upon visualizing the vorticity, we can observe that the area around the middle spherical concrete aggregate has potential for carbonation. However, more than 75 % of the total surface area of the surrounding spheres does not come into contact with the gas. We assume here that not all of the spheres would be completely carbonated. It is observed that much more time is taken to achieve thermal equilibrium in the whole system including the spherical concrete aggregates in both cases. The process of heat distribution is slower in the case of a bed of 81 spheres rather than that with a bed of 9 spheres. This is attributed to the fact that a part of the heat is absorbed by the spherical concrete aggregates, which means that the greater the number of spheres the longer it will take to reach thermal equilibrium in the system as shown in Figure 14.

D. Two-layered configuration of spherical concrete aggregates

In this section, we have configured them into a dual-layered arrangement with contact points in the view of exploring its influence on the gas flow dynamics as shown in Figure 15.

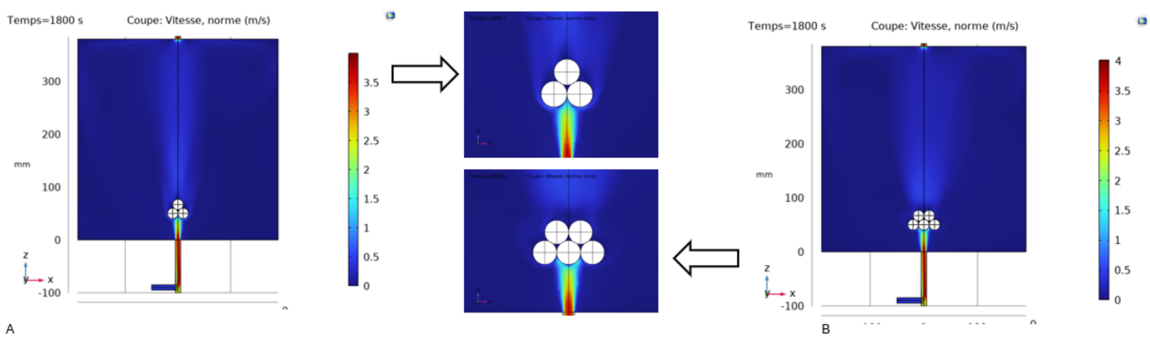

Figure 15 : A: Results of velocity distribution in reactor and around the spherical concrete aggregate for 3 spheres at t = 10 min with a zoom on the image beside B: Results of velocity distribution in reactor and around the spherical concrete aggregate for 5 spheres at t = 10 min with a zoom on the image beside.

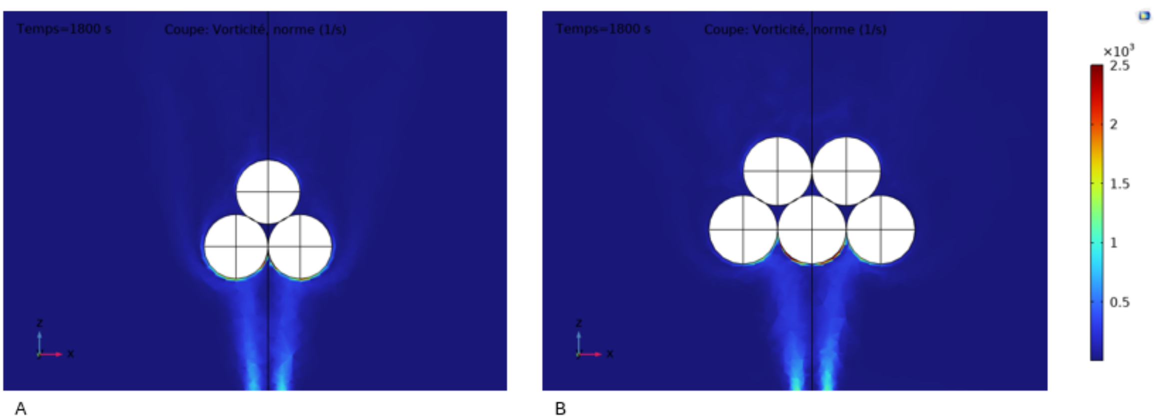

Figure 16 : Vorticity around the spherical concrete aggregates in 3 spheres and 5 spheres.

In Figure 15, the arrangement of the particles in a closed packed way significantly influences the flow pattern. As the gas flow through the spheres a turbulence is induced, creating fluctuations and non-uniformities in the flow pattern. The clustering and contact among the spheres hindered the passage of gas, resulting in the formation of dead zones at specific locations in both cases. So, visualizing the vorticity here is essential for a clearer depiction. In the first image in Figure 16, the vorticity is well distributed over the two first particles. However, for the spherical concrete aggregate above, approximately the entire surface is not in contact with the gas. The same scenario happens in the case with 5 spheres. Here also the two spherical concrete aggregates on top are deprived of any interaction with the gas. To summarize we have about over 75 % of the total surface area of certain spheres that are not even in contact with the gas. Thermal equilibrium was achieved in both scenarios by the end of the simulation. Unlike the simulation involving a bed of 81 spheres, where there was a notable temperature variance among the spherical concrete aggregates, in this case, the temperature difference among the spherical concrete aggregates is minimal. This can be attributed to the contact between the spherical concrete aggregates, thus facilitating heat propagation.

V. CONCLUSION

In conclusion, the simulations of the fluid flow and heat transfer in the reactor has provided valuable insights into its operational behavior and thermal characteristics. Several critical observations have been made regarding gas flow dynamics, temperature distribution and their potential implications for carbonation processes. We had a heterogeneity in the gas distribution around the concrete aggregate in the reactor as observed in the different scenarios that have been simulated. We had the emergence of unfavorable zones for carbonation called the dead zones usually behind the spherical concrete aggregates. The vorticity (presence of vortexes) may serve as an indicator of the carbonation zones; however, validation of this hypothesis is still pending through experimental testing. Regarding heat transfer, we were able to observe how the geometry influenced the distribution of heat in the reactor and among the spheres. We noticed a significant heterogeneity in the reactor across multiple particle simulations. This variability in particle number and arrangement can have profound effects on the fluids dynamics and heat transfer mechanisms, thus resulting in the overall reactor performance. These simulations not only contribute to our understanding of the reactor performance but also offer avenues for further exploration and optimization in industrial applications.

VI. PERSPECTIVE

This paper investigates the fluid flow dynamics and heat transfer phenomena within the reactor system and around the concrete aggregate. The subsequent phase involves integrating the diffusion-reaction process, specifically carbonation, into the numerical solution framework. This incorporation entails accounting for parameters like specific surface area, porosity, and chemical reactions (implementing a chemical module) within the computational model. This step is crucial for facilitating a comparative analysis with experimental findings.

REFERENCES

Gunzburger, M. D. (1996). Navier-Stokes equations for incompressible flows: Finite-element methods. *Handbook of Computational Fluid Mechanics*, 99–157. https://doi.org/10.1016/B978-012553010-1/50004-9

Jeong, J., Ramézani, H., Papadakis, V. G., Colin, J., & Izoret, L. (2022). On CO_2 sequestration in concrete aggregate via carbonation: simulation and experimental verification. *European Journal of Environmental and Civil Engineering*, *26*(12), 6076–6095. https://doi.org/10.1080/19648189.2021.1928555

Lombardi, L., Carnevale, E. A., & Pecorini, I. (2016). Experimental evaluation of two different types of reactors for CO_2 removal from gaseous stream by bottom ash accelerated carbonation. *Waste Management*, *58*, 287–298. https://doi.org/10.1016/j.wasman.2016.09.038

Minhua, Z., He, D., & Zhongfeng, G. (2019). A particle-resolved CFD model coupling reaction-diffusion inside fixed-bed reactor. *Advanced Powder Technology*, *30*(6), 1226–1238. https://doi.org/10.1016/j.apt.2019.03.019

Schmitt, L., Jeong, J., Potier, J. M., Izoret, L., Mai-Nh, J., Decousser, N., & Pernin, T. (2022). CARBON DIOXIDE BINDING ABILITY IN CONCRETES: METHODOLOGY AND MODELING. *Acta Polytechnica CTU Proceedings*, *33*, 546–551. https://doi.org/10.14311/APP.2022.33.0546

Schnabel, K., Brück, F., Mansfeldt, T., & Weigand, H. (2021). Full-scale accelerated carbonation of waste incinerator bottom ash under continuous-feed conditions. *Waste Management*, *125*, 40–48. https://doi.org/10.1016/j.wasman.2021.02.027

Torrenti, J. M., Amiri, O., Barnes-Davin, L., Bougrain, F., Braymand, S., Cazacliu, B., Colin, J., Cudeville, A., Dangla, P., Djerbi, A., Doutreleau, M., Feraille, A., Gueguen, M., Guillot, X., Hou, Y., Izoret, L., Jacob, Y. P., Jeong, J., Hiu Hoong, J. D. L., … Turcry, P. (2022). The FastCarb project: Taking advantage of the accelerated carbonation of recycled concrete aggregates. *Case Studies in Construction Materials*, *17*. https://doi.org/10.1016/j.cscm.2022.e01349

Wen, D., & Ding, Y. (2006). Heat transfer of gas flow through a packed bed. *Chemical Engineering Science*, *61*(11), 3532–3542. https://doi.org/10.1016/j.ces.2005.12.027